AIMS Mathematics, 10(7): 16746–16761.
DOI: 10.3934/math.2025752
Received: 19 June 2025
Revised: 10 July 2025
Accepted: 16 July 2025
Published: 25 July 2025

https://www.aimspress.com/journal/Math

Research article

Delay-dependent stability analysis of power system: A Monotone-Interval-Partition method for time-varying delays

Shihao Wang[1], Jin Yang[2,*], Yuejiang Wang[3], Qishui Zhong[1] and Kaibo Shi[4]

[1] School of Aeronautics and Astronautics, University of Electronic Science and Technology of China, Chengdu 611731, China

[2] School of Automation Engineering, University of Electronic Science and Technology of China, Chengdu 611731, China

[3] School of Government, University of Birmingham, Birmingham, B15 2TT, United Kingdom

[4] School of Electronic Information and Electrical Engineering, Chengdu University, Chengdu 610106, China

* **Correspondence:** Email: yangjin511325@163.com.

Abstract: This paper investigates the problem of a delay-dependent stability analysis in power systems, where the communication delay is modeled as a continuous, differentiable, aperiodic, and bounded function with constrained derivatives. First, a unified load frequency control system model is formulated that explicitly incorporates time-varying delays. Then, to more accurately address the delay characteristics, a monotonic interval partitioning strategy is introduced, which divides the delay trajectory into multiple segments based on its increasing or decreasing behavior. Each segment is associated with corresponding local extremal points of the delay function. Furthermore, to more effectively exploit the delay information, a new Lyapunov-Krasovskii functional (LKF) is developed, which integrates system states related to the local extremal values of the delay in each subinterval. By leveraging this LKF together with a convex combination method, less conservative stability conditions are derived. Finally, numerical case studies are presented to demonstrate the proposed approach's capability of enlarging the admissible delay bounds and validating its improved performance.

Keywords: power system; stability analysis; time-varying delays; monotone-interval-partition method
Mathematics Subject Classification: 93B52, 93C05

1. Introduction

Load frequency control (LFC) is a fundamental component in modern power system operation, designed to ensure that both the system frequency and power interchanges remain within prescribed bounds under varying load conditions [1–3]. Traditionally, LFC schemes have depended on dedicated and relatively stable communication infrastructures to relay real-time measurement signals and issue the corresponding control commands to generation units [4]. However, with the advent of deregulated electricity markets, the structure of power systems has become increasingly complex. The same communication networks that previously solely served for control purposes are now tasked with facilitating market-oriented interactions, such as the execution of bilateral contracts between generation companies and distribution companies. These dual-purpose communication channels are typically subject to congestion, variability, and other imperfections, which inevitably introduce non-negligible time delays into the control loop [5, 6]. Such delays, though often overlooked in early LFC designs, can severely compromise the system's ability to regulate the frequency, especially in fast-changing operational conditions. The dynamic response of the LFC system becomes slower and less accurate, potentially leading to frequency deviations that exceed the allowable thresholds. In this context, it becomes critically important to analyze and quantify the effects of communication-induced delays on the overall stability and performance of LFC strategies [7–9]. Therefore, a systematic investigation into the delay characteristics and their impact on frequency regulation is not only timely but also necessary to design robust LFC schemes capable of maintaining grid stability in the face of modern communication and market-driven complexities.

Given the inherently stochastic and time-varying characteristics of delays in real-world power systems, modern research trends have increasingly shifted toward time-domain analytical techniques. Among these, the Lyapunov-Krasovskii approach has proven particularly effective to derive delay-dependent stability conditions in the form of linear matrix inequalities (LMIs), which enable the determination of the system's maximum tolerable delay, commonly referred to as the delay margin [10, 11]. In [12], the stability of generalized neural networks with periodically time-varying delays was analyzed by constructing a refined Lyapunov-Krasovskii functional (LKF) that incorporated both the delay and its derivative through variation-dependent matrices. To further exploit the system structure, a novel looped functional based on neuronal activation was introduced, and enabled the relaxation of matrix definiteness conditions while utilizing the periodic and monotonic properties of the delay and activation functions. In the context of LFC with communication delays, more accurate delay margins can be obtained by designing refined LKFs and applying improved, less conservative inequality techniques to estimate their derivatives [13]. Despite the effectiveness of these methods, directly applying LMI-based criteria to the full-scale power system model often leads to significant computational challenges due to the high dimensionality of such models. This is particularly problematic in multi-area LFC frameworks, where the size and complexity of the system further increase. To mitigate this issue, recent studies, such as [14], have leveraged the structural sparsity of LFC models to simplify the computation. A common strategy involves constructing a transformation matrix that decomposes the system states into delay-sensitive and delay-insensitive components. This decomposition allows for the Lyapunov functional to be formulated over a reduced-order subsystem focused on the delay-dependent dynamics, thereby improving both the computational efficiency and the numerical tractability [15].

Dividing time-varying delays into multiple subintervals and designing LKFs tailored to each subinterval has emerged as an effective method to mitigate conservatism in stability analyses [16–18]. This approach enhances the resolution of delay-effect characterization by aligning the LKF structure more closely with the delay's local temporal behavior. A notable development for systems that experience periodic time-varying delays is the monotone delay interval technique in [17], which segments the delay trajectory into regions of consistent increase or decrease. Then, LKFs are then formulated over these monotonic intervals, thus allowing the derivation of the stability conditions with reduced conservatism by exploiting the inherent periodicity in the delay evolution. More recently, the concept of allowable delay set partitioning was proposed in [18], where a hybrid method integrates the set-based admissibility conditions with subinterval partitioning to further refine stability criteria. These frameworks represent significant advancements in the analysis of systems with structured delays, particularly when a delay variation follows a predictable pattern. In [19], a flexible fragmentation approach based on allowable delay sets was proposed for the passivity analysis of neural networks with time-varying delays. Based on this approach, a novel LKF was constructed by incorporating richer delay information. Subsequently, a relaxed passivity criterion was derived through the combination of integral inequalities and zero equations. To overcome the limitations, one promising strategy involves constructing LKFs that are responsive to extremal values within the delay trajectory. By capturing the system states that correspond to these locally critical points, one can potentially derive sharper and less conservative stability conditions. This novel methodology opens up new avenues for delay-dependent analyses in time-varying delays and paves the way for more generalizable LKF construction techniques suited to dynamically varying delay environments.

The main contributions of this work are summarized as follows:

(1) A unified modeling framework for LFC systems is constructed that explicitly incorporates time-varying communication delays. The delay is characterized as a bounded, differentiable, aperiodic, and continuous function with constrained derivatives. This modeling approach captures realistic delay dynamics, thus providing a solid foundation for accurate delay-dependent stability analyses.

(2) To better capture the characteristics of time-varying delays, a novel monotonic interval partitioning strategy is proposed. This method segments the delay trajectory based on its monotonicity, and identifies local extremal points within each interval. This refined partitioning allows for a more precise exploitation of delay variation patterns in the stability analysis.

(3) A new LKF is constructed to incorporate system states associated with local maximum and minimum delays within each subinterval. By leveraging this functional in combination with a convex combination approach, the paper derives delay-dependent stability conditions that are significantly less conservative. Numerical case studies confirm the effectiveness of the proposed method in enlarging admissible delay bounds and enhancing the system performance.

Notations: Let $\mathbb{N}+$ and $\mathbb{R}+$ represent the sets of positive integers and positive real numbers, respectively. The set $\mathbb{R}^n$ denotes the n-dimensional Euclidean space of real vectors, while $\mathbb{R}^{m\times n}$ stands for the space of real matrices with the dimension $m \times n$. For any matrix M, its transpose is denoted by M^{T}, and its inverse is written as M^{-1}. The symmetric part of M is defined as $\mathrm{He}(M) := M + M^{\mathrm{T}}$. $M > 0$ implies that M is symmetric and positive definite. Given $n \in \mathbb{N}_+$, for a sequence of vectors $\boldsymbol{m}_1, \ldots, \boldsymbol{m}_n$ and matrices $M_1, \ldots, M_n$, the concatenated column vector is expressed

as col$(\boldsymbol{m}_1, \ldots, \boldsymbol{m}_n) := [\boldsymbol{m}_1^{\mathrm{T}}, \ldots, \boldsymbol{m}_n^{\mathrm{T}}]^{\mathrm{T}}$, and the block-diagonal matrix formed by M_1 to M_n is denoted by diag$(M_1, \ldots, M_n)$.

2. System description and preliminaries

Figure 1 presents the LFC block diagram of a power system, as detailed in [20]. Drawing upon this configuration, the corresponding dynamic model for LFC is formulated as follows:

$$M\Delta\dot{f}(t) = -D\Delta f(t) + \Delta p_{\mathrm{t}}(t), \tag{2.1a}$$

$$T_{\mathrm{t}}\Delta\dot{p}_{\mathrm{t}}(t) = -\Delta p_{\mathrm{t}}(t) + \Delta p_{\mathrm{g}}(t), \tag{2.1b}$$

$$T_{\mathrm{g}}\Delta\dot{p}_{\mathrm{g}}(t) = -\frac{1}{R}\Delta f(t) - \Delta p_{\mathrm{g}}(t) + u(t), \tag{2.1c}$$

where $\Delta f(t)$, $\Delta p_{\mathrm{t}}(t)$, and $\Delta p_{\mathrm{g}}(t)$ denote the deviations in the system frequency, the mechanical power output of the generator, and the turbine valve position, respectively. The parameters M, D, T_{t}, T_{g}, and R represent the equivalent inertia constant, the damping factor, the turbine time constant, the governor time constant, and the droop characteristic of the governor, respectively.

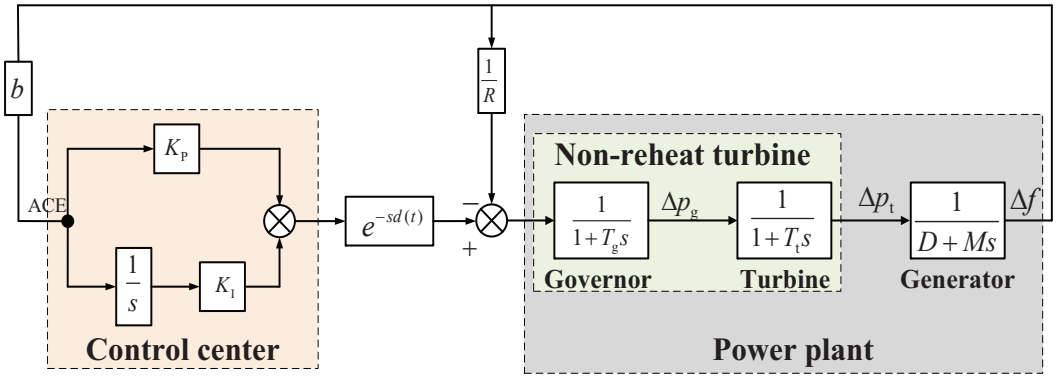

Figure 1. LFC model of power system.

$u(t)$ is the control input, which is designed as

$$u(t) = K_{\mathrm{P}}\mathrm{ACE}(t) + K_{\mathrm{I}}\int \mathrm{ACE}(t), \tag{2.2}$$

where K_{P} is the proportional control gain, K_{I} is the integral control gain, $\mathrm{ACE}(t) = b\Delta f(t)$ is the area control error, and b is the frequency bias coefficient.

Define the state vector as

$$\boldsymbol{x}(t) = \left[\Delta f^{\mathrm{T}}(t), \Delta p_{\mathrm{t}}^{\mathrm{T}}(t), \Delta p_{\mathrm{g}}^{\mathrm{T}}(t), \int \mathrm{ACE}^{\mathrm{T}}(t)\right]^{\mathrm{T}}.$$

Then, the dynamic model of the multi-area power system can be formulated as follows:

$$\begin{cases} \dot{\boldsymbol{x}}(t) = A\boldsymbol{x}(t) + A_{\mathrm{d}}\boldsymbol{x}(t - d(t)), \\ \boldsymbol{x}(t) = \boldsymbol{\theta}(t), \ t \in [-h_2, 0], \end{cases} \tag{2.3}$$

where

$$A = \begin{bmatrix} -\frac{D}{M} & \frac{1}{M} & 0 & 0 \\ 0 & -\frac{1}{T_t} & \frac{1}{T_t} & 0 \\ -\frac{1}{T_g R} & 0 & -\frac{1}{T_g} & 0 \\ b & 0 & 0 & 0 \end{bmatrix}, \ A_d = \begin{bmatrix} 0 & 0 & 0 & 0 \\ 0 & 0 & 0 & 0 \\ -\frac{bK_P}{T_g} & 0 & 0 & -\frac{K_I}{T_g} \\ 0 & 0 & 0 & 0 \end{bmatrix}.$$

$\boldsymbol{\psi}(t)$ represents the initial state, and the delay $d(t)$ is continuous, differentiable, and a bounded function constrained by

$$0 \le h_1 \le d(t) \le h_2, \quad -\mu \le \dot{d}(t) \le \mu, \tag{2.4}$$

with $h_1 \in \mathbb{R}_+$, $h_2 \in \mathbb{R}_+$, and $0 \le \mu \le 1$.

The aim of this paper is to seek an allowable upper bound of $d(t)$ (constrained by (2.4)), while ensuring the stability of system (2.3). The lemmas presented below will be utilized in the subsequent derivation of the stability criteria.

Lemma 2.1. *[21] Let $R > 0$ be a positive definite matrix, and suppose that the function $\boldsymbol{x}(s)$ is integrable over the interval $[\alpha_1, \alpha_2]$. Then, the following inequality holds:*

$$\alpha_{21} \int_{\alpha_1}^{\alpha_2} \dot{\boldsymbol{x}}^{\mathrm{T}}(s) R \dot{\boldsymbol{x}}(s)\, \mathrm{d}s \ge \boldsymbol{\phi}_1^{\mathrm{T}} R \boldsymbol{\phi}_1 + 3\boldsymbol{\phi}_2^{\mathrm{T}} R \boldsymbol{\phi}_2,$$

where $\boldsymbol{\phi}_1 = \boldsymbol{x}(\alpha_2) - \boldsymbol{x}(\alpha_1)$, and $\boldsymbol{\phi}_2 = \boldsymbol{x}(\alpha_2) + \boldsymbol{x}(\alpha_1) - 2\int_{\alpha}^{\beta} \frac{\boldsymbol{x}(s)}{\beta-\alpha}\, \mathrm{d}s$, $\alpha_{21} = \alpha_2 - \alpha_1$.

Lemma 2.2. *[22] Let $R \in \mathbb{R}^{p\times p}$ be a symmetric, and positive definite matrix. For any matrix $X \in \mathbb{R}^{2p\times q}$ that satisfies* $\mathrm{rank}(X) = 2p$ *and $2p \le q$, the following inequality holds for a differentiable function $\boldsymbol{x}(s)$ over the interval $[\alpha_1, \alpha_2]$:*

$$\int_{\alpha_1}^{\alpha_2} \dot{\boldsymbol{x}}^{\mathrm{T}}(s) R \dot{\boldsymbol{x}}(s)\, \mathrm{d}s \ge \mathrm{Sym}(X^{\mathrm{T}} Y) + (\beta - \alpha) X^{\mathrm{T}} \mathcal{R}^{-1} X,$$

where $Y = \mathrm{col}(\boldsymbol{x}(\alpha_2) - \boldsymbol{x}(\alpha_1), \boldsymbol{x}(\alpha_2) + \boldsymbol{x}(\alpha_1) - \frac{2}{\alpha_{21}} \int_{\alpha_1}^{\alpha_2} \boldsymbol{x}(s)\mathrm{d}s)$, $\alpha_{21} = \alpha_2 - \alpha_1$, and $\mathcal{R} = \mathrm{diag}\,(R,\ 3R)$.

3. Main results

In this section, an monotone interval partition (MIP) approach is introduced to address time-varying delays, with a primary focus on the delay-dependent stability analysis of a power system with time-varying delays.

3.1. Monotone-interval-partition approach

In what follows, we will divide the time-varying delay into several subintervals. Assume the time-varying delay $d(t)$ as continuous, differentiable, and bounded with restricted derivatives. According to its variation trend, it can be divided into $\bar{k}$, $\bar{k} \in \mathbb{N}_+$ monotone increasing and decreasing intervals. Figure 2 shows the schematic diagram of the time-varying delay $d(t)$.

In what follows, the time-varying delay $d(t)$ is partitioned into multiple subintervals based on its monotonic behavior. Assume that $d(t)$ is continuous, differentiable, bounded, and has a restricted

derivative. According to its variation pattern, $d(t)$ can be divided into $\bar{k}$, $\bar{k} \in \mathbb{N}_+$ monotonic segments, thereby alternating between increasing and decreasing intervals.

Specifically, for each monotonic segment, there exist time instants $t_{2k-1} < t_{2k}$, $k = 0, 1, \ldots, \bar{k}$, such that $d(t_{2k-1}) = h_1$ and $d(t_{2k}) = h_2$. Thus, $d(t)$ is monotonically increasing over $t \in [t_{2k-1}, t_{2k})$, and decreasing over $t \in [t_{2k}, t_{2k+1})$. Consequently, the derivative of the delay satisfies $\dot{d}(t) \in [0, \mu]$ in the increasing intervals and $\dot{d}(t) \in [-\mu, 0]$ in the decreasing intervals.

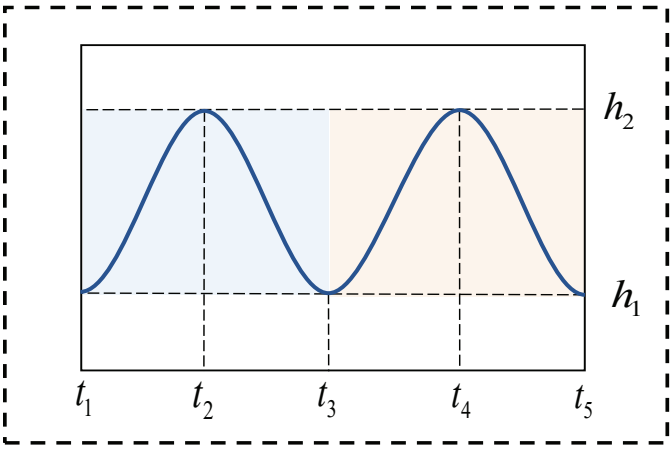

Figure 2. The schematic diagram of time-varying delay $d(t)$.

3.2. Stability analysis

In this section, a LKF is developed by integrating the system states associated with the boundary values of time-varying delays over each periodic subinterval and utilizing the MIP technique. Then, the Lyapunov stability theory is applied to analyze the stability of the power system. Consequently, a delay-dependent stability condition for system (2.3) is derived and formalized in Theorem 3.1.

For brevity, the following notations are defined:

$$
\begin{aligned}
d_1(t) =& d(t) - h_1, d_2(t) = h_2 - d(t),\\
\nu_1(t) =& \boldsymbol{x}(t-h_2) - \boldsymbol{x}(t-d(t)),\\
\nu_2(t) =& \boldsymbol{x}(t-d(t)) - \boldsymbol{x}(t-h_1),\\
\nu_3(t) =& \left[\boldsymbol{x}^{\mathrm{T}}(t) \quad \boldsymbol{x}^{\mathrm{T}}(t-h_1) \quad \boldsymbol{x}^{\mathrm{T}}(t-d(t)) \quad \boldsymbol{x}^{\mathrm{T}}(t-h_2)\right]^{\mathrm{T}},\\
\nu_4(t) =& \int_{t-h_1}^{t} \boldsymbol{x}(\rho)\mathrm{d}\rho, \nu_5(t) = \int_{t-d(t)}^{t-h_1} \boldsymbol{x}(\rho)\mathrm{d}\rho,\\
\nu_6(t) =& \int_{t-h_2}^{t-d(t)} \boldsymbol{x}(\rho)\mathrm{d}\rho,\\
\nu_7(t) =& \left[\dot{\boldsymbol{x}}^{\mathrm{T}}(t-h_1) \quad \dot{\boldsymbol{x}}^{\mathrm{T}}(t-d(t))\right]^{\mathrm{T}},\\
\nu_8(t) =& \left[\dot{\boldsymbol{x}}^{\mathrm{T}}(t-h_2) \quad \frac{1}{h_1}\nu_4^{\mathrm{T}}(t) \quad \frac{1}{d_1(t)}\nu_5^{\mathrm{T}}(t) \quad \frac{1}{d_2(t)}\nu_6^{\mathrm{T}}(t)\right]^{\mathrm{T}},\\
\boldsymbol{\xi}_1(t) =& \left[\nu_3^{\mathrm{T}}(t) \quad \nu_4^{\mathrm{T}}(t) \quad \nu_5^{\mathrm{T}}(t) \quad \nu_6^{\mathrm{T}}(t)\right]^{\mathrm{T}},\\
\boldsymbol{\xi}_2(\rho) =& \left[\boldsymbol{x}^{\mathrm{T}}(\rho)) \quad \dot{\boldsymbol{x}}^{\mathrm{T}}(\rho)\right]^{\mathrm{T}},
\end{aligned}
$$

$$\xi_3(t) = \begin{bmatrix} d_1(t)\nu_1^{\mathrm{T}}(t) & d_2(t)\nu_2^{\mathrm{T}}(t) \end{bmatrix}^{\mathrm{T}},$$
$$\xi_4(t) = \begin{bmatrix} \nu_3^{\mathrm{T}}(t) & \nu_4^{\mathrm{T}}(t) \end{bmatrix}^{\mathrm{T}}, \zeta(t) = \begin{bmatrix} \nu_3^{\mathrm{T}}(t) & \nu_7^{\mathrm{T}}(t) & \nu_8^{\mathrm{T}}(t) \end{bmatrix}^{\mathrm{T}},$$
$$\epsilon_i = \begin{bmatrix} 0_{n\times(l-1)n} & I_n & 0_{n\times(10-l)n} \end{bmatrix}, l = 1, \ldots, 10.$$

Theorem 3.1. *For a given $\mu \in [0, 1]$, $0 < h_1 < h_2$, the power system (2.3) is asymptotically stable if there are matrices $P > 0$, $Q_1 > 0$, $Q_2 > 0$, $Q_3 > 0$, $R_1 > 0$, $R_2 > 0$, U_{I_1}, U_{D_1}, U_{I_2}, U_{D_2}, W_{I_1}, W_{I_2}, W_{D_1}, W_{D_2}, and X_1, X_2, Y_1, Y_2, such that*

$$\begin{bmatrix} \bar{\Psi}_{\mathrm{I}}(h_1, \dot{d}(t)) & \sqrt{h_{21}}X_2^{\mathrm{T}} \\ * & -\hat{\mathcal{R}}_{\mathrm{I}_2}(\dot{d}(t)) \end{bmatrix}_{\dot{d}(t)\in[0,\mu]} < 0, \tag{3.1}$$
$$\begin{bmatrix} \bar{\Psi}_{\mathrm{I}}(h_2, \dot{d}(t)) & \sqrt{h_{21}}X_1^{\mathrm{T}} \\ * & -\hat{\mathcal{R}}_{\mathrm{I}_1}(\dot{d}(t)) \end{bmatrix}_{\dot{d}(t)\in[0,\mu]} < 0, \tag{3.2}$$
$$\begin{bmatrix} \bar{\Psi}_{\mathrm{D}}(h_1, \dot{d}(t)) & \sqrt{h_{21}}Y_2^{\mathrm{T}} \\ * & -\hat{\mathcal{R}}_{\mathrm{D}_2}(\dot{d}(t)) \end{bmatrix}_{\dot{d}(t)\in[-\mu,0]} < 0, \tag{3.3}$$
$$\begin{bmatrix} \bar{\Psi}_{\mathrm{D}}(h_2, \dot{d}(t)) & \sqrt{h_{21}}Y_1^{\mathrm{T}} \\ * & -\hat{\mathcal{R}}_{\mathrm{D}_1}(\dot{d}(t)) \end{bmatrix}_{\dot{d}(t)\in[-\mu,0]} < 0, \tag{3.4}$$

where $h_{21} = h_2 - h_1$,

$$\begin{aligned}
\bar{\Psi}_{\mathrm{I}}(d(t), \dot{d}(t)) =& \Psi_1(d(t), \dot{d}(t)) + \Psi_2(d(t), \dot{d}(t)) + \Psi_{\mathrm{I}}(d(t), \dot{d}(t)),\\
\bar{\Psi}_{\mathrm{D}}(d(t), \dot{d}(t)) =& \Psi_1(d(t), \dot{d}(t)) + \Psi_3(d(t), \dot{d}(t)) + \Psi_{\mathrm{D}}(d(t), \dot{d}(t)),\\
\Psi_1(d(t), \dot{d}(t)) =& \mathrm{He}(\Pi_1^{\mathrm{T}} P \Pi_2) + \Pi_3^{\mathrm{T}} Q_1 \Pi_3 + \Pi_4^{\mathrm{T}}(Q_2 - Q_1)\Pi_4\\
&+ (1 - \dot{d}(t))\Pi_5^{\mathrm{T}}(Q_3 - Q_2)\Pi_5 - \Pi_6^{\mathrm{T}} Q_3 \Pi_6\\
&+ h_1^2 \epsilon_0^{\mathrm{T}} R_1 \epsilon_0 + h_{21} \epsilon_0^{\mathrm{T}} R_2 \epsilon_0,\\
\Psi_2(d(t), \dot{d}(t)) =& -\Pi_{15}^{\mathrm{T}} \hat{\mathcal{R}}_1 \Pi_{15} + \mathrm{He}(X_1^{\mathrm{T}}\Pi_{16} + X_2^{\mathrm{T}}\Pi_{17}),\\
\Psi_3(d(t), \dot{d}(t)) =& -\Pi_{15}^{\mathrm{T}} \hat{\mathcal{R}}_1 \Pi_{15} + \mathrm{He}(Y_1^{\mathrm{T}}\Pi_{16} + Y_2^{\mathrm{T}}\Pi_{17}),\\
\Psi_{\mathrm{I}}(d(t), \dot{d}(t)) =& \mathrm{He}(\Pi_7^{\mathrm{T}} U_{\mathrm{I}_1} \Pi_8 + \Pi_9^{\mathrm{T}} U_{\mathrm{I}_1} \Pi_{10} + \Pi_{11}^{\mathrm{T}} U_{\mathrm{I}_2} \Pi_{12} + \Pi_{13}^{\mathrm{T}} U_{\mathrm{I}_2} \Pi_{14})\\
&- d_2(t)(\epsilon_5 W_{\mathrm{I}_1} \epsilon_5 - (1 - \dot{d}(t))\epsilon_7^{\mathrm{T}} W_{\mathrm{I}_1} \epsilon_7)\\
&+ d_1(t)((1 - \dot{d}(t))(\epsilon_6^{\mathrm{T}} W_{\mathrm{I}_2} \epsilon_6 - \epsilon_7 W_{\mathrm{I}_2} \epsilon_7)),\\
\Psi_{\mathrm{D}}(d(t), \dot{d}(t)) =& \mathrm{He}(\Pi_7^{\mathrm{T}} U_{\mathrm{D}_1} \Pi_8 + \Pi_9^{\mathrm{T}} U_{\mathrm{D}_1} \Pi_{10} + \Pi_{11}^{\mathrm{T}} U_{\mathrm{D}_2} \Pi_{12} + \Pi_{13}^{\mathrm{T}} U_{\mathrm{D}_2} \Pi_{14})\\
&- d_2(t)(\epsilon_5 W_{\mathrm{I}_1} \epsilon_5 - (1 - \dot{d}(t))\epsilon_7^{\mathrm{T}} W_{\mathrm{I}_1} \epsilon_7)\\
&+ d_1(t)((1 - \dot{d}(t))(\epsilon_6^{\mathrm{T}} W_{\mathrm{I}_2} \epsilon_6 - \epsilon_7 W_{\mathrm{I}_2} \epsilon_7)),\\
\hat{\mathcal{R}}_{\mathrm{D}_i}(\dot{d}(t)) =& \mathrm{diag}(R_2 - \dot{d}(t) W_{\mathrm{D}_i}, 3(R_2 - \dot{d}(t) W_{\mathrm{D}_i})),\\
\hat{\mathcal{R}}_{\mathrm{I}_i}(\dot{d}(t)) =& \mathrm{diag}(R_2 - \dot{d}(t) W_{\mathrm{I}_i}, 3(R_2 - \dot{d}(t) W_{\mathrm{I}_i})),
\end{aligned}$$

with

$$\begin{aligned}
\Pi_1 =& \mathrm{col}(\epsilon_1, \epsilon_2, \epsilon_3, \epsilon_4, h_1\epsilon_8, d_1(t)\epsilon_9, d_2(t)\epsilon_{10}),\\
\Pi_2 =& \mathrm{col}(\epsilon_0, \epsilon_5, (1 - \dot{d}(t))\epsilon_6, \epsilon_7, \epsilon_1 - \epsilon_2, \epsilon_2 - (1 - \dot{d}(t))\epsilon_3, (1 - \dot{d})\epsilon_3 - \epsilon_4),
\end{aligned}$$

$$
\begin{aligned}
\Pi_3 =&\mathrm{col}(\epsilon_1, \epsilon_0), \Pi_4 = \mathrm{col}(\epsilon_2, \epsilon_5), \Pi_5 = \mathrm{col}(\epsilon_3, \epsilon_6), \Pi_6 = \mathrm{col}(\epsilon_4, \epsilon_7),\\
\Pi_7 =&\mathrm{col}(\dot{d}(t)(\epsilon_4 - \epsilon_3) + d_1(t)(\epsilon_7 - (1 - \dot{d}(t))\epsilon_6)\\
&- \dot{d}(t)(\epsilon_3 - \epsilon_2) + d_2(t)(1 - \dot{d}(t))\epsilon_6 - \epsilon_5),\\
\Pi_8 =&\mathrm{col}(\epsilon_1, \epsilon_2, \epsilon_3, \epsilon_4, h_1\epsilon_8), \Pi_9 = \mathrm{col}(d_1(t)(\epsilon_4 - \epsilon_3), d_2(t)(\epsilon_3 - \epsilon_2)),\\
\Pi_{10} =&\mathrm{col}(\epsilon_0, \epsilon_5, (1 - \dot{d}(t))\epsilon_6, \epsilon_7, \epsilon_1 - \epsilon_2),\\
\Pi_{11} =&\epsilon_2 - (1 - \dot{d}(t))\epsilon_3, \Pi_{12} = d_2(t)\epsilon_{10}, \Pi_{13} = d_1(t)\epsilon_9,\\
\Pi_{14} =&(1 - \dot{d}(t))\epsilon_3 - \epsilon_4, \Pi_{15} = \mathrm{col}(\epsilon_1 - \epsilon_2, \epsilon_1 + \epsilon_2 - 2\epsilon_8),\\
\Pi_{16} =&\mathrm{col}(\epsilon_2 - \epsilon_3, \epsilon_2 + \epsilon_3 - 2\epsilon_9), \hat{\mathcal{R}}_1 = \mathrm{diag}(R_1, 3R_1),\\
\Pi_{17} =&\mathrm{col}(\epsilon_3 - \epsilon_4, \epsilon_3 + \epsilon_4 - 2\epsilon_{10}), \epsilon_0 = A\epsilon_1 + A_\mathrm{d}\epsilon_3.
\end{aligned}
$$

Proof. The LKF candidate is chosen as

$$
V(t) = \begin{cases} V_\mathrm{c}(t) + V_\mathrm{I}(t), & t \in [t_{2k-1}, t_{2k}) \\ V_\mathrm{c}(t) + V_\mathrm{D}(t), & t \in [t_{2k}, t_{2k+1}) \end{cases}, \tag{3.5}
$$

where

$$
\begin{aligned}
V_\mathrm{c}(t) =&\boldsymbol{\xi}_1^{\mathrm{T}}(t)P\boldsymbol{\xi}_1(t) + \int_{t-h_1}^{t} \boldsymbol{\xi}_2^{\mathrm{T}}(s)Q_1\boldsymbol{\xi}_2(s)\mathrm{d}s + \int_{t-d(t)}^{t-h_1} \boldsymbol{\xi}_2^{\mathrm{T}}(s)Q_2\boldsymbol{\xi}_2(s)\mathrm{d}s\\
&+ \int_{t-h_2}^{t-d(t)} \boldsymbol{\xi}_2^{\mathrm{T}}(s)Q_3\boldsymbol{\xi}_2(s)\mathrm{d}s + h_1\int_{-h_1}^{0}\int_{t+\rho}^{t} \dot{\boldsymbol{x}}^{\mathrm{T}}(s)R_1\dot{\boldsymbol{x}}(s)\mathrm{d}s\mathrm{d}\rho\\
&+ \int_{-h_2}^{-h_1}\int_{t+\rho}^{t} \dot{\boldsymbol{x}}^{\mathrm{T}}(s)R_2\dot{\boldsymbol{x}}(s)\mathrm{d}s\mathrm{d}\rho,
\end{aligned} \tag{3.6}
$$

$$
\begin{aligned}
V_\mathrm{I}(t) =&2\boldsymbol{\xi}_3^{\mathrm{T}}(t)U_{\mathrm{I}_1}\boldsymbol{\xi}_4(t) + 2\nu_5^{\mathrm{T}}(t)U_{\mathrm{I}_2}\nu_6(t) + (d(t) - d(t_{2k}))\int_{t-d(t)}^{t-d(t_{2k-1})} \dot{\boldsymbol{x}}^{\mathrm{T}}(s)W_{\mathrm{I}_1}\dot{\boldsymbol{x}}(s)\mathrm{d}s\\
&+ (d(t) - d(t_{2k-1}))\int_{t-d(t_{2k})}^{t-d(t)} \dot{\boldsymbol{x}}^{\mathrm{T}}(s)W_{\mathrm{I}_2}\dot{\boldsymbol{x}}(s)\mathrm{d}s,
\end{aligned} \tag{3.7}
$$

$$
\begin{aligned}
V_\mathrm{D}(t) =&2\boldsymbol{\xi}_3^{\mathrm{T}}(t)U_{\mathrm{D}_1}\boldsymbol{\xi}_4(t) + 2\nu_5^{\mathrm{T}}(t)U_{\mathrm{D}_2}\nu_6(t) + (d(t) - d(t_{2k}))\int_{t-d(t)}^{t-d(t_{2k+1})} \dot{\boldsymbol{x}}^{\mathrm{T}}(s)W_{\mathrm{D}_1}\dot{\boldsymbol{x}}(s)\mathrm{d}s\\
&+ (d(t) - d(t_{2k+1}))\int_{t-d(t_{2k})}^{t-d(t)} \dot{\boldsymbol{x}}^{\mathrm{T}}(s)W_{\mathrm{D}_2}\dot{\boldsymbol{x}}(s)\mathrm{d}s.
\end{aligned} \tag{3.8}
$$

Note that

$$
\lim_{t\to t_{2k+1}^-} V(t) = \lim_{t\to t_{2k+1}^+} V(t),
$$

which confirms the continuity of the LKF (3.5) over time. Furthermore, $P > 0$, $Q_i > 0$, and $R_i > 0$ guarantee $V(t) > 0$. Subsequently, the calculation of $\dot{V}(t)$ along the trajectory of system (2.3) yields

$$
\dot{V}_\mathrm{c}(t) = \boldsymbol{\zeta}^{\mathrm{T}}(t)\Psi_1(d(t), \dot{d}(t))\boldsymbol{\zeta}(t) + F_1 + F_2, \tag{3.9}
$$

$$
\dot{V}_\mathrm{I}(t) = \boldsymbol{\zeta}^{\mathrm{T}}(t)\Psi_2(d(t), \dot{d}(t))\boldsymbol{\zeta}(t) + F_3 + F_4, \tag{3.10}
$$

where

$$F_1 = -h_1 \int_{t-h_1}^{t} \dot{\boldsymbol{x}}^{\mathrm{T}}(s) R_1 \dot{\boldsymbol{x}}(s) \mathrm{d}s, \tag{3.11}$$

$$F_2 = -\int_{t-h_2}^{t-h_1} \dot{\boldsymbol{x}}^{\mathrm{T}}(s) R_2 \dot{\boldsymbol{x}}(s) \mathrm{d}s, \tag{3.12}$$

$$F_3 = \dot{d}(t) \int_{t-d(t)}^{t-h_1} \dot{\boldsymbol{x}}^{\mathrm{T}}(s) W_{\mathrm{I}_1} \dot{\boldsymbol{x}}(s) \mathrm{d}s, \tag{3.13}$$

$$F_4 = \dot{d}(t) \int_{t-h_2}^{t-d(t)} \dot{\boldsymbol{x}}^{\mathrm{T}}(s) W_{\mathrm{I}_2} \dot{\boldsymbol{x}}(s) \mathrm{d}s. \tag{3.14}$$

Furthermore, F_i is estimated as follows by applying Lemmas 2.1 and 2.2:

$$F_1 \leq -\boldsymbol{\zeta}^{\mathrm{T}}(t)(\Pi_{15}^{\mathrm{T}} \hat{\mathcal{R}}_1 \Pi_{15}) \boldsymbol{\zeta}(t), \tag{3.15}$$

$$\begin{aligned} \sum_{i=2}^{4} F_i \leq & \boldsymbol{\zeta}^{\mathrm{T}}(t)(+\mathrm{He}(X_1^{\mathrm{T}} \Pi_{16} + X_2^{\mathrm{T}} \Pi_{17})) \boldsymbol{\zeta}(t) + \boldsymbol{\zeta}^{\mathrm{T}}(t)((d(t) - h_1) X_1^{\mathrm{T}} \hat{\mathcal{R}}_{\mathrm{I}_1}^{-1}(\dot{d}(t)) X_1 \\ & + (h_2 - d(t)) X_2^{\mathrm{T}} \hat{\mathcal{R}}_{\mathrm{I}_2}^{-1} X_2) \boldsymbol{\zeta}(t), \end{aligned} \tag{3.16}$$

where $\hat{\mathcal{R}}_{\mathrm{I}_i}(\dot{d}(t)) = \mathrm{diag}(R_2 - \dot{d}(t) W_{\mathrm{I}_i}, 3(R_2 - \dot{d}(t) W_{\mathrm{I}_i}))$.

If (3.9)–(3.16) are combined, then

$$\begin{aligned} \dot{V}(t) \leq & \boldsymbol{\zeta}^{\mathrm{T}}(t) \Psi_{\mathrm{I}}(d(t), \dot{d}(t)) \boldsymbol{\zeta}(t) + \boldsymbol{\zeta}^{\mathrm{T}}(t)((d(t) - h_1) X_1^{\mathrm{T}} \hat{\mathcal{R}}_{\mathrm{I}_1}^{-1}(\dot{d}(t)) X_1 \\ & + (h_2 - d(t)) X_2^{\mathrm{T}} \hat{\mathcal{R}}_{\mathrm{I}_2}^{-1} X_2) \boldsymbol{\zeta}(t). \end{aligned} \tag{3.17}$$

Assume that the conditions $\bar{\Psi}_{\mathrm{I}}(h_1, \dot{d}(t)) + h_{21} X_2^{\mathrm{T}} \hat{\mathcal{R}}_{\mathrm{I}_2}^{-1} X_2 < 0$ and $\bar{\Psi}_{\mathrm{I}}(h_2, \dot{d}(t)) + h_{21} X_1^{\mathrm{T}} \hat{\mathcal{R}}_{\mathrm{I}_1}^{-1} X_1 < 0$ hold for $\dot{d}(t)(t) \in [0, \mu]$, which are equivalent to (3.20) and (3.21), respectively. Then, it follows that there exists a constant $\alpha_1 \in \mathbb{R}^+$ such that $\dot{V}(t) < -\alpha_1 |\boldsymbol{x}(t)|^2$.

For the interval $t \in [t_{2k}, t_{2k+1})$, where $\dot{d}(t) \in [-\mu, 0]$, a similar reasoning yields:

$$\begin{aligned} \dot{V}(t) \leq & \boldsymbol{\zeta}^{\mathrm{T}}(t) \Psi_{\mathrm{D}}(d(t), \dot{d}(t)) \boldsymbol{\zeta}(t) + \boldsymbol{\zeta}^{\mathrm{T}}(t)((d(t) - h_1) X_1^{\mathrm{T}} \hat{\mathcal{R}}_{\mathrm{D}_1}^{-1}(\dot{d}(t)) X_1 \\ & + (h_2 - d(t)) X_2^{\mathrm{T}} \hat{\mathcal{R}}_{\mathrm{D}_2}^{-1} X_2) \boldsymbol{\zeta}(t). \end{aligned} \tag{3.18}$$

Under conditions (3.22) and (3.23), there exists a scalar $\alpha_2 > 0$ such that $\dot{V}(t) < -\alpha_2 |\boldsymbol{x}(t)|^2$ for $t \in [t_{2k}, t_{2k+1})$.

Combining the two cases, it can be concluded that $\dot{V}(t) < -\alpha_m |\boldsymbol{x}(t)|^2$ on $t \in [t_0, +\infty)$, where $\alpha_m = \min(\alpha_1, \alpha_2)$. Integrating the inequality, we have

$$V(t) - V(0) < -\alpha_m \int_{t_0}^{t} |\boldsymbol{x}(s)|^2 \mathrm{d}s. \tag{3.19}$$

Given that $V(t_{2k-1}) \geq V(t) \geq V(t_{2k+1}) \geq \lambda_{\min}(P) |\boldsymbol{x}(t_{2k+1})|^2$ for $t \in [t_{2k-1}, t_{2k+1})$, it follows that $V(t)$ remains positive and bounded over $[t_0, +\infty)$. Therefore, by applying Barbalat's Lemma, the system state satisfies $\boldsymbol{x}(t) \to 0$ as $t \to +\infty$. □

Remark 3.1. *It is important to note that the pair* $(d(t), \dot{d}(t))$ *lies within the set* $S = [h_1, h_2] \times [-\mu, \mu]$*, which forms a rectangular polytope in the delay–derivative space. To further exploit the structural properties of the time-varying delay and its rate of change, this domain is partitioned into two distinct regions:* $S_1 = [h_1, h_2]\times[-\mu, 0]$ *and* $S_2 = [h_1, h_2]\times[0, \mu]$*, which correspond to decreasing and increasing delay intervals, respectively. To accurately reflect the dynamic behavior of the system under these two delay trends, separate sets of Lyapunov matrices are independently selected for each region, that is, different LKFs are constructed for cases where* $(d(t), \dot{d}(t))$ *belongs to* S_1 *and* S_2*. This delay-interval-specific treatment enables the functional to more effectively capture localized characteristics of the delay. As a result, the proposed Lyapunov approach—based on the segmentation of the delay domain according to its monotonic behavior—significantly contributes to mitigating the conservatism often observed in conventional stability analyses. By tailoring the functional to each monotone delay region, the derived stability conditions become more accurate and less restrictive, thus leading to a broader admissible delay margin and an enhanced analytical precision.*

Algorithm 1 : An algorithm for seeking the allowable h_2.

Input:
The change rate of time-varying delay: $\mu \in [0, 1)$;
The lower bound of time-varying delay: $h_1 > 0$;
The maximal value of h_1: $h_1^{\max} > 0$;
The change step of h_1: Δh_1;
The change step of h_2: Δh_2;
The change step of μ: $\Delta\mu$;
Output: The allowable h_2;

```
for h1 = 0 : Δh1 : h1^max
    for μ = 0 : Δμ : 1
        Solve the LMIs in Theorem 3.1;
        if (3.20)-(3.23) are feasible, then
            h2 = h2 + Δh2;
        else
            h2 = h2 − Δh2;
            Output h2 and break.
        end
    end
end
```

Remark 3.2. *Unlike conventional Lyapunov functional designs, the proposed framework does not impose the non-negativity constraint on the intermediate Lyapunov terms* $V_{\mathrm{I}}(t)$ *and* $V_{\mathrm{D}}(t)$*, that is, it does not require* $V_{\mathrm{I}}(t) \geq 0$ *and* $V_{\mathrm{D}}(t) \geq 0$ *to hold for all t. This strategic relaxation significantly reduces the conservatism typically associated with traditional stability criteria, thus allowing for a more flexible and less restrictive condition derivation. Specifically, consider the time interval* $t \in [t_{2k-1}, t_{2k})$*. Given the assumptions* $V(t_{2k-1}) \geq 0$*,* $V(t_{2k}) \geq 0$*, and the negative definiteness of the Lyapunov derivative* $\dot{V}(t) \leq -\alpha_m|\boldsymbol{x}(t)|^2$*, it directly follows that the Lyapunov functional is non-increasing over this interval.*

As a result, the value of $V(t)$ remains bounded within $V(t_{2k-1}) \geq V(t) \geq V(t_{2k}) \geq 0$. An analogous conclusion can be drawn for the subsequent interval $t \in [t_{2k}, t_{2k+1})$, where one similarly obtains $V(t_{2k}) \geq V(t) \geq V(t_{2k+1}) \geq 0$. By piecing together these inequalities over successive intervals, it is ensured that the Lyapunov functional $V(t)$ remains non-negative for all $t \geq t_0$, even though its individual components V_{I} and V_{D} may not be strictly positive. This property plays a crucial role in facilitating the application of Barbalat's lemma and ultimately guarantees the asymptotic stability of the system.

Remark 3.3. *To simplify the formulation and analysis, the time-varying delay $d(t)$ is assumed as a periodic function, that is, the maximum variation rates of the time-delay in the increasing and decreasing intervals are identical. Each period of the time-varying delay consists of one monotonic increasing interval and one monotonic decreasing interval. This assumption facilitates a more concise representation of the proposed method. However, it is worth noting that the methodology is not limited to this simplified scenario. In [23], a discrete-time looped functional and a refined allowable delay set were proposed to model cyclically varying delays. The delay considered in this study exhibits a cyclic pattern, thereby alternating between rising and falling phases within predetermined upper and lower bounds. The proposed approach can be readily extended to handle more general cases that involve multiple increasing and decreasing monotonic segments within each delay period, thus broadening its applicability to a wider range of practical systems.*

If the LKF is selected as $V_{\mathrm{c}}(t)$, without accounting for the monotonic behavior of the time-varying delay, then a corresponding stability criterion can still be derived, as stated in the following corollary.

Corollary 3.1. *For a given $\mu \in [0, 1]$, $0 < h_1 < h_2$, the power system (2.3) is asymptotically stable if there are matrices $P > 0$, $Q_1 > 0$, $Q_2 > 0$, $Q_3 > 0$, $R_1 > 0$, $R_2 > 0$, X and Y such that*

$$\begin{bmatrix} \bar{\Psi}(h_1, \dot{d}(t)) & \sqrt{h_{21}} X_2^{\mathrm{T}} \\ * & -\hat{\mathcal{R}}_2 \end{bmatrix}_{\dot{d}(t)\in[0,\mu]} < 0, \tag{3.20}$$

$$\begin{bmatrix} \bar{\Psi}(h_2, \dot{d}(t)) & \sqrt{h_{21}} X_2^{\mathrm{T}} \\ * & -\hat{\mathcal{R}}_2 \end{bmatrix}_{\dot{d}(t)\in[0,\mu]} < 0, \tag{3.21}$$

$$\begin{bmatrix} \bar{\Psi}(h_1, \dot{d}(t)) & \sqrt{h_{21}} X_2^{\mathrm{T}} \\ * & -\hat{\mathcal{R}}_2 \end{bmatrix}_{\dot{d}(t)\in[-\mu,0]} < 0, \tag{3.22}$$

$$\begin{bmatrix} \bar{\Psi}(h_2, \dot{d}(t)) & \sqrt{h_{21}} X_2^{\mathrm{T}} \\ * & -\hat{\mathcal{R}}_2 \end{bmatrix}_{\dot{d}(t)\in[-\mu,0]} < 0, \tag{3.23}$$

where $h_{21} = h_2 - h_1$,

$$\begin{aligned}
\bar{\Psi}(d(t), \dot{d}(t)) =& \Psi_1(d(t), \dot{d}(t)) + \Psi_2(\dot{d}(t)), \\
\Psi_1(d(t), \dot{d}(t)) =& \mathrm{He}(\Pi_1^{\mathrm{T}} P \Pi_2) + \Pi_3^{\mathrm{T}} Q_1 \Pi_3 + \Pi_4^{\mathrm{T}} (Q_2 - Q_1) \Pi_4 + (1 - \dot{d}(t)) \Pi_5^{\mathrm{T}} (Q_3 - Q_2) \Pi_5 \\
& - \Pi_6^{\mathrm{T}} Q_3 \Pi_6 + h_1^2 \epsilon_0^{\mathrm{T}} R_1 \epsilon_0 + h_{21} \epsilon_0^{\mathrm{T}} R_2 \epsilon_0, \\
\Psi_2(\dot{d}(t)) =& - \Pi_7^{\mathrm{T}} \hat{\mathcal{R}}_1 \Pi_7 + \mathrm{He}(X_1^{\mathrm{T}} \Pi_8 + X_2^{\mathrm{T}} \Pi_9), \\
\hat{\mathcal{R}}_2 =& \mathrm{diag}(R_2, 3R_2),
\end{aligned}$$

with

$$\Pi_1 = \mathrm{col}(\epsilon_1, \epsilon_2, \epsilon_3, \epsilon_4, h_1 \epsilon_8, d_1(t) \epsilon_9, d_2(t) \epsilon_{10}),$$

$$\Pi_2 = \text{col}(\epsilon_0, \epsilon_5, (1-\dot{d}(t))\epsilon_6, \epsilon_7, \epsilon_1-\epsilon_2, \epsilon_2-(1-\dot{d}(t))\epsilon_3, (1-\dot{d})\epsilon_3-\epsilon_4),$$
$$\Pi_3 = \text{col}(\epsilon_1, \epsilon_0), \Pi_4 = \text{col}(\epsilon_2, \epsilon_5), \Pi_5 = \text{col}(\epsilon_3, \epsilon_6), \Pi_6 = \text{col}(\epsilon_4, \epsilon_7),$$
$$\Pi_7 = \text{col}(\epsilon_1-\epsilon_2, \epsilon_1+\epsilon_2-2\epsilon_8), \Pi_8 = \text{col}(\epsilon_2-\epsilon_3, \epsilon_2+\epsilon_3-2\epsilon_9),$$
$$\Pi_9 = \text{col}(\epsilon_3-\epsilon_4, \epsilon_3+\epsilon_4-2\epsilon_{10}), \epsilon_0 = A\epsilon_1 + A_d\epsilon_3, \hat{\mathcal{R}}_1 = \text{diag}(R_1, 3R_1).$$

4. Examples

A numerical example is provided in this section to demonstrate the effectiveness and advantages of the proposed MIP approach. This example serves to validate the theoretical results and highlight the improvements in the stability analysis achieved by applying the MIP method.

Set $K_P = 0.15$ and $K_I \in \{0.05, 0.10, 0.15\}$, with the corresponding parameters of (2.3) provided in Table 1. By applying Theorem 3.1 with $\mu = 0.5$ and $h_1 = 0.5$, the allowable upper bound h_2 is determined. The obtained results are presented in Table 2. It can be observed that the maximum values of h_2 obtained from Theorem 3.1 are greater than those reported in [24], thus demonstrating that the proposed LKFs result in a less conservative stability criterion.

Table 1. Parameters of system (2.3).

M	D	T_t	T_g	R	b
10.00	1.00	0.30	0.10	0.05	21.00

Table 2. The allowable upper bound h_2 for different K_I.

Methods	$[K_P, K_I]$		
	[0.10, 0.05]	[0.10, 0.10]	[0.10, 0.15]
Corollary 1 [24]	13.77	10.98	8.58
Theorem 1 [24]	13.90	11.09	8.61
Corollary 3.1	14.05	11.37	8.68
Theorem 3.1	15.21	12.55	8.74

Let the initial condition be specified as

$$\boldsymbol{\phi}(t) = \begin{bmatrix} 0.42 & 0.33 & 0.25 & 0.35 \end{bmatrix}^T.$$

The time-varying delay is defined by the expression

$$d(t) = \mid a(t) \mid \cos^2(t) + b(t),$$

where $a(t)$ and $b(t)$ are continuous functions of time, constrained such that $\mid a(t) \mid + b(t) \in [h_1, h_2]$, thus ensuring the total delay remains within a prescribed interval.

To simulate the dynamic response of system (2.3), the control parameters are set as $[K_P, K_I] = [0.10, 0.05]$. The resulting state trajectories are illustrated in Figures 3 and 4, where Figure 3 corresponds to the system evolution with a delay-free scenario and Figure 4 reflects the system evolution with time-varying delays. By comparing the two, it is evident that the inclusion of time-varying delays leads to more pronounced fluctuations in the state variables, thus highlighting the destabilizing impact of delays on the system's transient behavior.

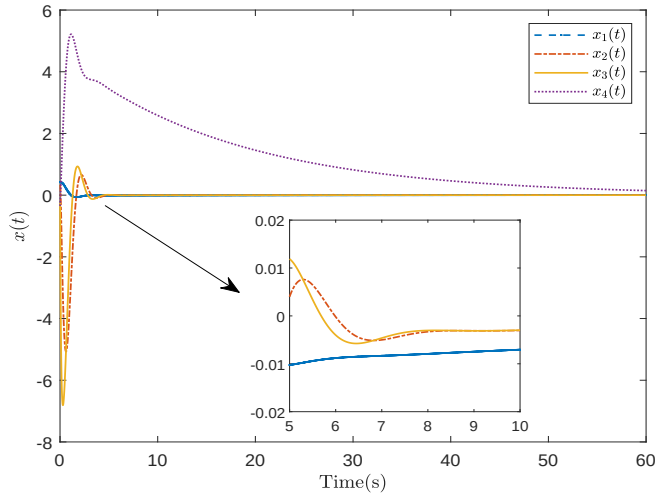

Figure 3. States trajectories of power system (2.3) without delay.

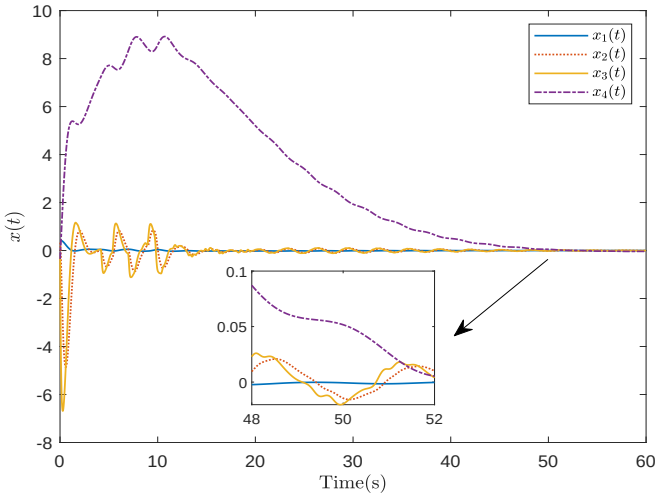

Figure 4. States trajectories of power system (2.3) with time-varying delays.

5. Conclusions

This paper has investigated the delay-dependent stability analysis problem of power systems, where the communication delay has been modeled as a bounded, continuous, differentiable, and aperiodic function with constrained derivatives. A unified model for the load frequency control system has been formulated to explicitly account for time-varying delays. To better reflect the characteristics of the delay, a monotonic interval partitioning strategy has been proposed, which segments the delay trajectory into subintervals based on its increasing or decreasing trends, each associated with local extremal values. To fully utilize the information within these subintervals, a novel LKF has been constructed by incorporating system states that correspond to the local maximum and minimum delays. Based on this functional and a convex combination technique, less conservative delay-

dependent stability criteria have been derived. Numerical examples have been carried out, confirming that the proposed method effectively enlarges the admissible delay bounds. In future research, the proposed framework can be extended to accommodate more complex system settings, such as multi-area LFC structures with heterogeneous communication delays. Moreover, incorporating stochastic or random delay variations into the modeling process could provide a more realistic basis for practical implementation. Another promising direction involves integrating event-triggered or data-driven control strategies into the proposed LKF design to further enhance the system efficiency and reduce the communication burden under limited bandwidth conditions.

Author contributions

Shihao Wang: Contributed to the study's conceptual design, developed the methodology, and prepared the original draft of the manuscript; Jin Yang: Provided critical revisions and editorial input and was responsible for securing funding for the project; Yuejiang Wang: Performed formal data analysis and contributed to experimental investigation; Qishui Zhong: Supplied key research resources and carried out validation of the results; Kaibo Shi: Assisted in formal analysis and experimental procedures. All authors have read and approved the final version of the manuscript for publication.

Use of Generative-AI tools declaration

The authors declare they have not used Artificial Intelligence (AI) tools in the creation of this article.

Acknowledgments

This work was supported by Sichuan Science and Technology Plan under Grants 2024ZDZX0040 and 2025ZNSFSC1512.

Conflict of interest

The authors declare no conflicts of interest.

References

1. X. C. Shangguan, Y. He, C. K. Zhang, L. Jin, W. Yao, L. Jiang, et al., Control performance standards-oriented event-triggered load frequency control for power systems under limited communication bandwidth, *IEEE Trans. Control Syst. Techn.*, **30** (2022), 860–868. https://doi.org/10.1109/TCST.2021.3070861
2. R. Zhu, C. Huang, S. Deng, Y. Li, Detection of false data injection attacks based on kalman filter and controller design in power system LFC, *J. Phys. Conf. Ser.*, **1861** (2021), 012120. https://doi.org/10.1088/1742-6596/1861/1/012120
3. N. Vafamand, M. M. Arefi, M. H. Asemani, T. Dragicevic, Decentralized robust disturbance-observer based lfc of interconnected systems, *IEEE Trans. Ind. Electron.*, **69** (2022), 4814–4823. https://doi.org/10.1109/TIE.2021.3078352

4. M. M. Hossain, C. Peng, H. T. Sun, S. Xie, Bandwidth allocation-based distributed event-triggered LFC for smart grids under hybrid attacks, *IEEE Trans. Smart Grid*, **13** (2022), 820–830. https://doi.org/10.1109/TSG.2021.3118801

5. G. Zhang, J. Li, O. Bamisile, Y. Xing, D. Cai, Q. Huang, An H_∞ load frequency control scheme for multi-area power system under cyber-attacks and time-varying delays, *IEEE Trans. Power Syst.*, **38** (2023), 1336–1349. https://doi.org/10.1109/TPWRS.2022.3171101

6. L. Yang, T. Liu, D. J. Hill, Decentralized event-triggered frequency regulation for multi-area power systems, *Automatica*, **126** (2021), 109479. https://doi.org/10.1016/j.automatica.2020.109479

7. T. N. Pham, S. Nahavandi, L. V. Hien, H. Trinh, K. P. Wong, Static output feedback frequency stabilization of time-delay power systems with coordinated electric vehicles state of charge control, *IEEE Trans. Power Syst.*, **32** (2017), 3862–3874. https://doi.org/10.1109/TPWRS.2016.2633540

8. S. Saxena, E. Fridman, Event-triggered load frequency control via switching approach, *IEEE Trans. Power Syst.*, **35** (2020), 4484–4494. https://doi.org/10.1109/TPWRS.2020.2999488

9. J. Yang, Q. Zhong, X. Liu, K. Shi, A. M. Y. M. Ghias, Z. Y. Dong, Decentralized periodic event-triggered load frequency control for multiarea power systems, *IEEE Trans. Syst. Man Cybern. Syst.*, **55** (2025), 1020–1030. https://doi.org/10.1109/TSMC.2024.3493102

10. R. Olfati-Saber, R. M. Murray, Consensus problems in networks of agents with switching topology and time-delays, *IEEE Trans. Autom. Control*, **49** (2004), 1520–1533. https://doi.org/10.1109/TAC.2004.834113

11. J. Yang, Q. Zhong, H. Liang, K. Shi, Z. Y. Dong, Distributed observer-based dynamic-memory event-triggered security control for interconnected linear systems, *IEEE Trans. Autom. Sci. Eng.*, **22** (2025), 9958–9969. https://doi.org/10.1109/TASE.2024.3515148

12. Y. Chen, Y. Li, G. Chen, New results on stability analysis for a class of generalized delayed neural networks, *Appl. Math. Comput.*, **469** (2024), 128529. https://doi.org/10.1016/j.amc.2024.128529

13. M. J. Park, O. M. Kwon, J. H. Ryu, Generalized integral inequality: Application to time-delay systems, *Appl. Math. Lett.*, **77** (2018), 6–12. https://doi.org/10.1016/j.aml.2017.09.010

14. M. R. Chen, G. Q. Zeng, X. Q. Xie, Population extremal optimization-based extended distributed model predictive load frequency control of multi-area interconnected power systems, *J. Franklin Inst.*, **355** (2018), 8266–8295. https://doi.org/10.1016/j.jfranklin.2018.08.020

15. X. C. Shang-Guan, Y. He, C. Zhang, L. Jiang, J. W. Spencer, M. Wu, Sampled-data based discrete and fast load frequency control for power systems with wind power, *Appl. Energy*, **259** (2020), 114202. https://doi.org/10.1016/j.apenergy.2019.114202

16. W. Wang, W. M. Wang, H. B. Zeng, Stability analysis of systems with cyclical delay via an improved delay-monotonicity-dependent Lyapunov functional, *J. Franklin Inst.*, **360** (2023), 99–108. https://doi.org/10.1016/j.jfranklin.2022.11.032

17. H. B. Zeng, Y. He, K. L. Teo, Monotone-delay-interval-based Lyapunov functionals for stability analysis of systems with a periodically varying delay, *Automatica*, **138** (2022), 110030. https://doi.org/10.1016/j.automatica.2021.110030

18. Y. Chen, H. B. Zeng, Y. Li, Stability analysis of linear delayed systems based on an allowable delay set partitioning approach, *Automatica*, **163** (2024), 111603. https://doi.org/10.1016/j.automatica.2024.111603

19. Y. Chen, C. Lu, X. M. Zhang, Allowable delay set flexible fragmentation approach to passivity analysis of delayed neural networks, *Neurocomputing*, **629** (2025), 129730. https://doi.org/10.1016/j.neucom.2025.129730

20. H. B. Zeng, S. J. Zhou, X. M. Zhang, W. Wang, Delay-dependent stability analysis of load frequency control systems with electric vehicles, *IEEE Trans. Cybern.*, **52** (2022), 13645–13653. https://doi.org/10.1109/TCYB.2022.3140463

21. P. Park, W. I. Lee, S. Y. Lee, Auxiliary function-based integral inequalities for quadratic functions and their applications to time-delay systems, *J. Franklin Inst.*, **352** (2015), 1378–1396. https://doi.org/10.1016/j.jfranklin.2015.01.004

22. H. B. Zeng, X. G. Liu, W. Wang, A generalized free-matrix-based integral inequality for stability analysis of time-varying delay systems, *Appl. Math. Comput.*, **354** (2019), 1–8. https://doi.org/10.1016/j.amc.2019.02.009

23. W. H. Chen, C. K. Zhang, R. W. Chen, K. Y. Xie, Y. He, H. B. Zeng, A discrete-time looped functional approach and its application to discrete-time systems with cyclically varying delays, *Sci. China Inf. Sci.*, **68** (2025), 182204. https://doi.org/10.1007/s11432-024-4220-6

24. C. K. Zhang, F. Long, Y. He, W. Yao, L. Jiang, M. Wu, A relaxed quadratic function negative-determination lemma and its application to time-delay systems, *Automatica*, **113** (2020), 108764. https://doi.org/10.1016/j.automatica.2019.108764

AIMS Press